

Stirred, not shaken: Star cluster survival in the slingshot scenario

D. R. Matus Carrillo,^{1*} M. Fellhauer,¹ T. C. N. Boekholt,² A. Stutz,¹
and M. C. B. Morales Inostroza¹

¹ *Departamento de Astronomía, Universidad de Concepción, Casilla 160-C, Concepción, Chile*

² *Rudolf Peierls Centre for Theoretical Physics, Clarendon Laboratory, Parks Road, Oxford, OX1 3PU, UK*

Accepted XXX. Received YYY; in original form ZZZ

ABSTRACT

We investigate the effects of an oscillating gas filament on the dynamics of its embedded stellar clusters. Motivated by recent observational constraints, we model the host gas filament as a cylindrically symmetrical potential, and the star cluster as a Plummer sphere. In the model, the motion of the filament will produce star ejections from the cluster, leaving star cluster remnants that can be classified into four categories: a) Filament Associated clusters, which retain most of their particles (stars) inside the cluster and inside the filament; b) destroyed clusters, where almost no stars are left inside the filament, and there is no surviving bound cluster; c) ejected clusters, that leave almost no particles in the filament, since the cluster leaves the gas filament; and d) transition clusters, corresponding to those clusters that remain in the filament, but that lose a significant fraction of particles due to ejections induced by filament oscillation. Our numerical investigation predicts that the Orion Nebula Cluster is in the process of being ejected, after which it will most likely disperse into the field. This scenario is consistent with observations which indicate that the Orion Nebula Cluster is expanding, and somewhat displaced from the Integral Shaped Filament ridgeline.

Key words: stars: kinematics and dynamics– ISM: individual objects – methods: numerical

1 INTRODUCTION

The majority of stars form in filamentary gas structures in molecular clouds (André et al. 2010). Star clusters are no exception. In the early phases, the star clusters are gas-dominated (Lada & Lada 2003), and the gas is arranged in simple structured filaments that can be approximately modelled as cylinders (Stutz & Gould 2016). The key question here is how the gas properties may affect the embedded cluster properties and dynamics. The nearest (~ 400 pc, Kounkel et al. 2018; Stutz et al. 2018), and arguably best-studied embedded cluster is the Orion Nebula Cluster (ONC, Hillenbrand 1997; Hillenbrand & Hartmann 1998), which is forming within the massive Integral shaped Filament (ISF, Bally et al. 1987). These star and gas structures are embedded in the massive ($M \sim 10^5 M_\odot$) Orion A molecular cloud (OMC, Bally et al. 1987).

The OMC has a mass of $1.1 \times 10^5 M_\odot$ (Hartmann & Burkert 2007), distributed along an extension of ~ 90 pc (Großschedl et al. 2018). This structure is composed of many smaller filaments and clumps, with over 100 individual condensations identified (Bally et al. 1987). Of these structures, one of the most striking is the ISF, named as such thanks to its distinctive shape, which corresponds to the northern part of the OMC.

In the middle of the ISF, the ONC is forming, as mentioned above. The ONC is the brightest and most prominent stellar structure in Orion A, and it's nebulosity is visible with the naked eye. The estimated ONC total mass is $\sim 1000 M_\odot$ (Da Rio et al. 2012; Stutz 2018). The mean stellar mass is $\sim 0.7 M_\odot$ (Hillenbrand 1997; Take-

mura et al. 2021), with individual stellar masses that range from below the hydrogen burning limit to $\sim 33 M_\odot$ (Hillenbrand 1997; Balega et al. 2014). In isolation, a bound star cluster will evolve towards a spherical shape, due to the gravitational interaction of the stars. The ONC, being partially embedded inside the ISF, is not isolated, and its stars are moving under the influence of the gas. As a consequence, it is not circularly symmetrical, and it is elongated similar to the gas distribution in the region (Hillenbrand & Hartmann 1998), with an ellipticity between 0.3 to 0.5 (Hillenbrand & Hartmann 1998; Da Rio et al. 2014).

Some authors (e.g. Da Rio et al. 2017; Kim et al. 2019) claim that the velocity dispersion of the stars of the ONC indicate that the cluster is in a virialized state, or slightly supervirial. On the other hand, others (e.g. Jones & Walker 1988; Fűrész et al. 2008; Tobin et al. 2009; Da Rio et al. 2014; Stutz 2018; Theissen et al. 2022) claim that the system is not yet virialized, and is either in expansion (Jones & Walker 1988; Swiggum et al. 2021), or the dynamics are still dominated by the gas (Fűrész et al. 2008; Tobin et al. 2009; Stutz 2018). Numerical experiments (e.g. Kroupa et al. 1999, 2001; Scally et al. 2005) indicate that the best fit models for the ONC corresponds to models in expansion, where the gas was either absent (Kroupa et al. 1999; Scally et al. 2005), or removed shortly after the beginning of the simulation (Kroupa et al. 2001), in which they find that the ONC might evolve to a Pleiades-like cluster after ejecting 2/3 of the initial stars. Proszkow et al. (2009) find that the observed properties of the ONC can be explained by assuming a nonspherical cluster, where stars have subvirial velocities.

Observation of protostars and pre-main-sequence stars in the ISF show that while protostars are located right on top of the ridgeline of

* E-mail: dimatus@udec.cl (DMC)

the filament, pre-main-sequence stars are symmetrically distributed around the filament (Stutz & Gould 2016; Beccari et al. 2017; Kainulainen et al. 2017; Stutz 2018). Other star forming regions, such as NGC1333, also show younger stars near the gas filaments, while older stars are distributed more uniformly within the gas cloud (Foster et al. 2015; Hacar et al. 2017). The radial velocity of the stars relative to the gas is also different for the younger and older populations, where protostars have radial velocities close to the velocity of the gas, with a low velocity dispersion. Meanwhile, the pre-main-sequence stars have a larger radial velocity dispersion, of the order of, or even larger than, the velocity dispersion of the gas (Stutz & Gould 2016). A larger distance from the ridgeline of the filament, plus a larger velocity relative to the gas, implies that the older stars have more kinetic energy than the protostars. The gas of the ISF presents undulations, not only in space, which gives the filament its name, but also in velocity (González Lobos & Stutz 2019). The regularity of these undulations suggests that the filament is being subjected to strong transverse forces (Stutz & Gould 2016; Stutz et al. 2018).

To explain these observations, Stutz & Gould (2016) proposed a scenario where the gas of the ISF oscillates. Stutz & Gould (2016) named this scenario “the Slingshot”, in which the movement of the filament is injecting energy into the stellar system, increasing the velocity and spread of the older stars. In this scenario, the filament is moving; inside the filament the gas starts to collapse to form a protostar. Since the protostar is forming from the filament, it has a low velocity relative to the filament. Once the protostar accretes enough mass, it decouples from the gas. In this decoupled state, when the filament starts to decelerate, the star is not able to stay in the ridgeline of the filament, and is ejected; that is, it is not the stars who leave the filament, but the filament is leaving the stars (Stutz & Gould 2016).

Stutz & Gould (2016) note that, at the scale of the filament as a whole, the ratio of gravitational and magnetic energy indicates that the magnetic fields are supercritical, while at scales of ~ 1 pc, the fields are subcritical. This balance between the magnetic and the gravitational field would allow the ISF not only to suffer violent periodic perturbations, which would create the conditions needed to trigger the formation of clusters and eject stars, but also to survive said perturbations.

Stutz (2018) assumed a spherically symmetric density distribution to model the ONC stars. Their best match was a Plummer model (Plummer 1911), with scale radius $R_{pl} = 0.36$ pc, and a central density of $5755 M_{\odot} \text{pc}^{-3}$. They determined that the gravity of the gas dominates over the gravity of the stars at all radii, with the exception of $r = 0.36$ pc, which corresponds to the scale radius of the ONC. At that point, the gravity of the stars has the same magnitude as the gravity of the gas. They also estimate the crossing time of the cluster, finding a value of ~ 0.55 Myr, very similar to the estimate of the gas filament motion (0.6 Myr, Stutz & Gould 2016). The fact that the scale length of the cluster has the same value as the distance at which the cluster gravity and the gas gravity have equal magnitude, suggests that the filament regulates the development of the structural parameters of the cluster.

Schleicher & Stutz (2018) show that, when taking into consideration the effects of a magnetic field on the gas, the system evolves to a state where gravitational, rotational and magnetic energy are comparable. Under these conditions, any perturbation in the filament will give rise to periodic oscillations. When applying these results to the ISF, they obtain an oscillation period of 2.9 Myr, comparable to the timescales estimated by Stutz & Gould (2016) and Boekholt et al. (2017).

The slingshot scenario was tested by Boekholt et al. (2017). They

test if an oscillating gas filament is able to reproduce some of the observed properties predicted by the slingshot. They represent the gas filament by using a cylindrically symmetric, analytical density profile with a polytrope-like softening. This filament is constantly accelerating, with the position of the central part of the filament moving along the x -axis following a sinusoidal function. Embedded in the oscillating potential, they place a string of point mass particles, with small deviation from the centre of the filament and zero initial velocity. As the filament moves, so do the particles in the string of stars. They found that an initially narrow distribution of stars can be dynamically broadened by the oscillation of the filament. The fraction of particles ejected by the filament at each oscillation depends on the maximum acceleration of the motion. When the fraction of particles is equal on both sides of the filament, the particles have a non zero velocity with respect to the filament.

In an effort to explain the ONC, Kroupa et al. (2018) also provide an alternate idea for how the ONC formed. In their scenario, very young clusters with masses in the range $300\text{--}2000 M_{\odot}$ are able to suppress stellar formation due to the presence of O stars which ionise the gas and reduce the gas inflow, eject the ionising stars via dynamical interactions, and then restart the star formation phase, producing populations with different ages. With the expulsion of the gas, the cluster can also expand, explaining the different spatial distributions of these populations. Another explanation for the extended distribution of the stars in the ISF comes from three body interactions between stars in the ONC. Three body systems are unstable, and sooner or later, one of the bodies will be ejected (Valtonen & Karttunen 2006). Reipurth et al. (2010) use three body interactions with a background potential to study the evolution of primordial binaries within star forming clouds. They subtract mass from the background potential to simulate the destruction of cloud cores. While the triple system manage to eject stars outside the cloud core, to distances comparable to the radial extent of the ONC, the escaping stars do not have the high velocities observed in the ISF.

Following Boekholt et al. (2017), in this work we continue the exploration of the effects of the Slingshot scenario on embedded star clusters like the ONC. In this work we replace the string of stars with a spherical cluster of stars, representing the ONC, and study the effects of the filament, both static and in oscillation, on the dynamical evolution, and possible destruction, of the cluster.

This paper is structured as follows. In Section 2 we show the filament model used, the methods that we employ to generate the star cluster, their initial masses and radii, and the software used to run the simulations. Section 3 covers the case for a static filament. In Section 4 we explore the effects of the oscillating filament on clusters of different masses and radii. Finally, in Section 5 we present a summary of the results and our conclusions.

2 METHOD

In this section we describe the code used for the simulations (Section 2.1). Then we continue with a description of the model we use for the filament (Section 2.2) and the star cluster (Section 2.3). For the filament we assume a softened power law cylindrical density profile and sinusoidal oscillations. For the star cluster we assume a spherical Plummer density profile, and vary the mass and radius. We finish this section with a description of the initial conditions and parameters used in the simulations (Section 2.4).

2.1 AMUSE and BRIDGE

Our experiment requires a numerical framework capable of solving the N-body (where $N = 1000$) cluster problem self-consistently with a time-dependent background potential (the filament, Section 2.2). The Astrophysical Multi-purpose Software Environment (AMUSE; McMillan et al. 2012; Pelupessy et al. 2013; Portegies Zwart et al. 2013; Portegies Zwart & McMillan 2018) allows us to accomplish this. AMUSE is the astrophysical implementation of MUSE (Portegies Zwart et al. 2009), a software framework that has the capability to combine computational tools for different physical domains, allowing for self-consistent multi-physics simulations. For this project, we use PH4 (McMillan et al. 2012; Portegies Zwart & Bédorf 2014), a 4th order Hermite predictor-corrector N-body code, written in C++, to update the position and velocities of the particles. PH4 can be compiled with GPU support, which we use to speed up our simulations.

We also need a way to account for the effects of the gas filament. The filament is represented as a analytical background potential (Section 2.2). Instead of adding the background potential directly in the source code of PH4, we use the BRIDGE method (Fujii et al. 2007). BRIDGE provides a way to couple different codes to obtain a self-consistent simulation. In our case, BRIDGE couples PH4 with the background potential, so that the particles in the cluster will move under the gravity of the filament. To avoid numerical effects, the time-step of the simulation must be chosen carefully. A small value will give an increased precision when calculating the sum of the forces acting on a particle, but at the cost of increased CPU time. The BRIDGE timestep, effectively the timestep of the cluster-filament system, is set to 100 yr. This timestep is equivalent to $6 \times 10^{-3} t_{\text{cross, min}}$, where $t_{\text{cross, min}}$ is the smallest crossing time between the models of Table 1.

The total time of the simulation, T_{sim} , is two times the oscillation period, or 2 Myr, whichever is larger. This allows us to study the effects of at least one full oscillation cycle on the cluster. For simulations regarding the static filament case, the system is let to evolve for a total of 2 Myr. To study the evolution of the system, a series of snapshots are taken at regular intervals. Each snapshot is taken every $T_{\text{sim}}/500$, for a total of 500 snapshots per simulation. Numerical studies of fragmentation in turbulent gas clouds (e.g. Seifried & Walch 2015; Clarke et al. 2017) show that filaments with line mass density comparable to the ISF fragment and form stars on timescales of a few tenths of Myr. This will change the density profile of the gas filament, reducing the effect of the Slingshot on the cluster. Although we run our simulations for times of up to 10 Myr, much longer than the fragmentation timescale, we are interested in exploring the oscillation parameter space in the idealized case where the filament exists for several Myr, which include periods that are longer than the lifetime of real filaments. As we will see below (Sections 4.2 to 4.5), the effects of the moving filament on the cluster happen within the first 1/4 oscillation, so this length of time will be enough to eject, or destroy, the young cluster.

2.2 The filament

Based on dust maps of Stutz & Kainulainen (2015) and the analysis published by Stutz & Gould (2016), Stutz (2018) calculated a mass density profile of the ISF at the position of the ONC. They show that the gas density and gravitational potential of the filament within $0.05 < r < 8.5$ pc follows a power law profile with a power law index of $\gamma = 0.225$. Even though the potential is well behaved at $r = 0$, the gravitational acceleration and volume density diverge. Since the density profile must flatten at some point, we follow the method

developed by Boekholt et al. (2017), to model the filament as a cylindrically symmetrical potential. This potential extends to infinity along the z axis, with the profile being constant along said axis, and a radial dependence that follows a power law with a polytrope-like softening:

$$\rho(r)_{\text{model}} = \rho_0 \left[1 + \left(\frac{r}{D} \right)^2 \right]^{\frac{\gamma-2}{2}} \quad (1)$$

$$\Lambda(r)_{\text{model}} = \Lambda_0 \left\{ \left[1 + \left(\frac{r}{D} \right)^2 \right]^{\frac{\gamma}{2}} - 1 \right\} \quad (2)$$

$$g(r)_{\text{model}} = \begin{cases} -\frac{2G\Lambda(r)}{r} \hat{r} & r > 0 \\ 0\hat{r} & r = 0 \end{cases} \quad (3)$$

$$r^2 = (x_{\text{fil}} - x)^2 + (y_{\text{fil}} - y)^2 \quad (4)$$

where $\rho_0 = 7.6 \times 10^{10} \text{ M}_{\odot} \text{ pc}^{-3}$ is the density at the filament axis, D is the softening radius, γ is the power law of the gas profile, and $\Lambda_0 = 2\pi\rho_0 D^2 \gamma^{-1} = 53.07 \text{ M}_{\odot} \text{ pc}^{-1}$ is the line mass density. The D parameter regulates the curvature of the model. When $r \gg D$, our models converge to the power law observed by Stutz & Gould (2016). We adjust the value of the softening radius D so that the difference between the value given by our model (Equation 2) and the value of the line mass density at 8.5 pc, observed by Stutz & Gould (2016), is less than 10%. We set the value of the softening parameter to $D = 5 \times 10^{-6} \text{ pc}$. While this value is small, on the order of 1 AU, a larger value would increase the curvature of the profile within the region observed by Stutz & Gould (2016). The quantities x_{fil} and y_{fil} correspond to the position of the ridgeline, and are defined below (Equations 5 and 6). These profiles are valid within the few inner parsecs from the filament centre. The enclosed mass, given by the density profile, will grow without bounds, reaching an infinite mass when integrated to infinity.

The observations from Stutz & Gould (2016) extends to ~ 8.5 pc and do not show a cut-off. Since most of our stellar interactions occur within that radius, the cut-off in the density profile will be of limited importance in our result and it is not included in the model. The softening radius D , central density ρ_0 and power law of the gas profile γ have the same value for all simulations.

The slingshot scenario indicates that the ISF is a standing wave (Stutz et al. 2018; González Lobos & Stutz 2019). To mimic the motion of the filament, we use a sinusoidal function to determine the position of the gas potential ridgeline:

$$x_{\text{fil}}(t) = A \sin\left(\frac{2\pi}{P} t\right) \quad (5)$$

$$y_{\text{fil}}(t) = 0 \quad (6)$$

where A corresponds to the amplitude of the oscillation and P is the period of the oscillation. From the values A and P , we can also obtain the maximum velocity and maximum acceleration of the filament:

$$v_{\text{max}} = \frac{2\pi}{P} A \quad (7)$$

$$a_{\text{max}} = \left(\frac{2\pi}{P}\right)^2 A \quad (8)$$

For small values of A , or large values of P , this model reduces to the static filament model. Even though the movement of the filament might be more complex in reality, this function is the simplest model that can be analysed in detail. The values of the parameters A and P are shown in Table 1.

Table 1. Parameters of the Plummer models (Plummer radius, Plummer mass and relaxation time of both an isolated Plummer sphere and a Plummer sphere embedded in the filament), plus oscillation parameters range used in the simulations and mass ratio between the filament and the cluster, at the Plummer radius. From these model sets, model D (highlighted with a star) uses the mass and radius of the ONC derived from [Stutz \(2018\)](#). We use 10 values for the oscillation amplitude, and 10 values for the oscillation period, within the respective range, for a total of 100 filaments per model.

Model	R_{pl} [pc]	M_{pl} [M_{\odot}]	$t_{\text{relax,nogas}}$ [Myr]	$t_{\text{relax,gas}}$ [Myr]	Amplitude range [pc]	Period range [Myr]	$\Lambda(R_{\text{pl}})/M_{\text{cl}}(R_{\text{pl}})$
A	0.1	250	2.54	1.73	0.05 - 5.0	0.5 - 5.0	4.97
B	0.1	500	1.79	1.42	0.25 - 5.0	0.5 - 5.0	2.48
C	0.1	1000	1.26	1.21	0.5 - 4.0	0.5 - 5.0	1.24
D*	0.36	1124	8.17	5.41	1.0 - 2.5	0.5 - 3.5	1.52

2.3 The Cluster

The star cluster is represented by a Plummer sphere ([Plummer 1911](#)) with 1000, equal mass ($m_{\text{particle}} = M_{\text{pl}}/1000$), particles.

We use different values for the Plummer radius R_{pl} and the Plummer mass M_{pl} to study the way different clusters react to the motion of the filament (Table 1). For all models, the mass of the filament dominates over the mass of the cluster at a distance of $r = R_{\text{pl}}$ (Table 1). Furthermore, we use a fixed particle number to prevent the low mass models from having too few particles, and for the high mass models to use too much computer time.

The addition of an external potential will affect the dynamics of the cluster. In isolation, a Plummer model will keep its spherically symmetric distribution ([Binney & Tremaine 2008](#)), but our cylindrical potential will prevent this. Due to the symmetry of the potential, the gas will exert a force only in the direction perpendicular to the filament, i. e. in the $x - y$ plane. To prevent a collapse of the cluster in the direction perpendicular to the filament, we increase the $x - y$ velocities of the particles, adding enough energy to the stars so that the combined system is stable and not collapsing. The magnitude of the augmented velocity for a given particle is drawn from the distribution function of a Plummer sphere ([Binney & Tremaine 2008](#)). Instead of using the escape velocity from an isolated Plummer sphere at the position of the particle, we use difference between the potential of the filament-cluster system at the position of the star and at a distance of $5 R_{\text{pl}}$, effectively increasing the maximum velocity that the stars can have. This way, particles will have enough energy to reach, at most, a distance of $5 R_{\text{pl}}$; any star that has moved beyond this limit must have had its energy increased via dynamical interactions with the filament, other stars of the cluster, or both. The new velocity v_{mod} is assigned to the particle, keeping the original z component of the velocity, and modifying the x and y components of the velocity so that the magnitude of the new velocity is v_{mod} .

2.4 Initial Conditions

To explore the effects of an oscillating gas potential on the dynamics of an embedded star cluster, we use clusters with different Plummer radii and total masses. A total of 15 combinations of Plummer radii and total masses for the clusters (Table 1) were used. In all cases, the initial position of the centre of mass of the cluster corresponds with the ridgeline of the filament. The clusters start with zero initial velocity. Before the filament begins to move, the cluster is left to evolve inside a static filament for a period equivalent to 3 times the crossing time of a Plummer sphere with the same total mass and Plummer radius than the model.

Sets A,B,C and D explore the effects of the oscillating potential on the centre, by using filaments with different amplitude and period (Section 4). Each set uses ten, equally spaced, values for the ampli-

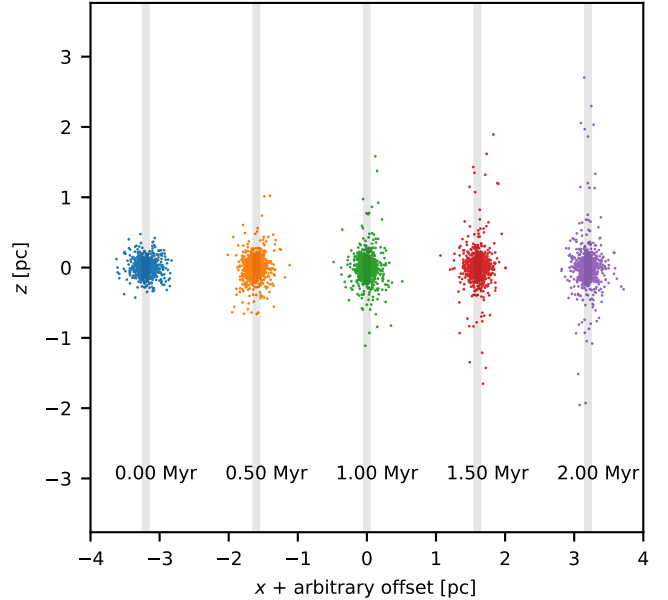


Figure 1. Snapshots of a cluster with $R_{\text{pl}} = 0.1$ pc, $M_{\text{pl}} = 500 M_{\odot}$ inside a static filament. Due to the symmetry of the potential, the particles of the cluster are free to move along the filament, following “corkscrew” orbits around the ridgeline. As a result, the cluster evolves to a non-spherical equilibrium shape.

tude and period of the oscillation, for a total of 100 filaments per cluster model.

3 STATIC FILAMENT

Setting the amplitude of the oscillation to $A = 0$ pc, we obtain the static filament case. Although the ISF is not static ([Stutz & Gould 2016](#)), we consider first the case with $A = 0$ pc to demonstrate the stability of the cluster, and to provide a benchmark for the evolution of the cluster without gas motions. We study the evolution of a cluster in a static filament by using models with different Plummer masses ($100 M_{\odot}$, $500 M_{\odot}$ and $2000 M_{\odot}$) and Plummer radius of 0.1 pc (Table 2). The gas mass enclosed within the Plummer radius is, according to Equation 2 is $\Lambda(0.1 \text{ pc})_{\text{model}} = 440 M_{\odot}$. We evolve the clusters inside the filament for 2 Myr.

Due to the symmetry of the potential, the gas filament only produces forces parallel to the $x - y$ plane, therefore, the particles are free to move in the z direction, with “corkscrew” orbits around the filament. These “corkscrew” orbits may have observational effects on proper motion and radial velocity data of young stars in gas filaments. This has the effect of extending the particle distribution (Figure 1),

Table 2. Plummer models used for the static filament.

M_{pl} [M_{\odot}]	R_{pl} [pc]	Simulation time [Myr]
100	0.1	2.0
500	0.1	2.0
2000	0.1	2.0

transforming the initially spherical cluster to a system elongated in the direction parallel to the filament. Nonetheless, the cluster is still attracting these particles, so they will eventually stop moving away from the cluster and will fall back. Particles with $v > v_{\text{esc,cl}}$, which are unbound from the cluster but still bound to the filament, will keep moving along the filament without falling back into the cluster.

The stability of the cluster can be seen by plotting the Lagrangian radii of the cluster (Figure 2, left panels). They show almost no change during the 2 Myr that the simulation last. The velocity adjustment (Section 2.3) will also increase the velocity dispersion in the x and y axis, while also preserving the original value in the z direction. Figure 2, right panel, shows the difference between the velocity dispersion in these two directions. For less dense clusters, the ratio σ_x/σ_z is larger than for more massive clusters. This difference tells us that clusters with shallower potentials need a larger velocity boost to prevent collapse due to the filament. On the other hand, the cluster with $M_{\text{pl}} = 2000M_{\odot}$ has similar velocity dispersion in all axes, meaning that a more dense object does not need a velocity boost to prevent contraction.

4 OSCILLATING FILAMENT

Motivated by the observational evidence outline above (Section 1), we aim to study the effect of a time-dependent potential on the cluster structure, specifically that of an ‘‘oscillating filament’’. One of the effects of the oscillation of the filament on the cluster will be the loss of mass from the cluster, so we try to quantify the degree of mass loss and particle ejection. The models that we use for the filament (Section 2.2) do not include a cutoff radius for the gas mass and, therefore, there is no well-defined escape velocity for the particles. Instead, we use a practical criterion that consists of particle displacement from the cluster centre or potential ridgeline. We define a particle as escaped from the filament if $r > 5 R_{\text{pl}}$ from the centre of the filament, or escaped from the cluster if $r > 5 R_{\text{pl}}$ from the centre of density (Casertano & Hut 1985) of the cluster. This distance is chosen since no particles are located beyond that radius at time $t = 0$. Once the filament has completed one full oscillation, we count the number of particles that are inside these limits.

Figure 3 shows the retained particle fractions of a cluster with a total mass of $M_{\text{pl}} = 250 M_{\odot}$ and Plummer radius $R_{\text{pl}} = 0.1$ pc. These values correspond to 100 realizations of Model A in Table 1, each inside a filament with different values of oscillation period and oscillation amplitude. Top panel shows the fraction of particles left inside the filament at the end of one oscillation, while the bottom panel shows the fraction of particles in the cluster. In both panels, the color code indicates the fraction of particles left in the respective structure at the end of the first oscillation, with contours for 75%, 50% and 25% of the initial number of particles. For small amplitudes and large periods, most of the particles remain inside the filament (top) and the cluster (bottom). As the maximum velocity of the filament increases, a larger fraction of particles are ejected from the system, up to the point where almost all the particles have left the filament, and

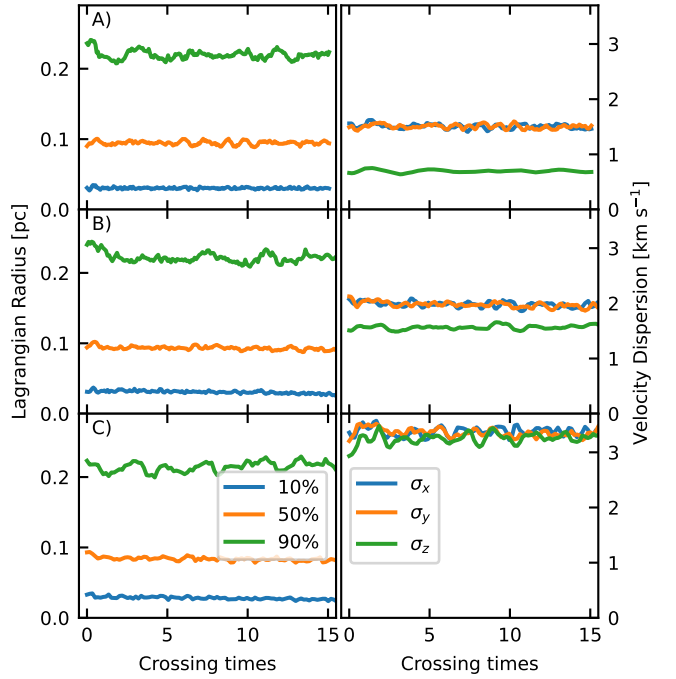


Figure 2. Lagrangian radii (left) and Velocity dispersion (right) for clusters inside a static filament. All panels correspond to clusters with the same Plummer radius ($R_{\text{pl}} = 0.1$ pc), but different masses: A) $100 M_{\odot}$, B) $500 M_{\odot}$, and C) $2000 M_{\odot}$. For panels in the left column, the colours indicate the amount of mass enclosed within the respective radius: blue lines for 10% of the total mass, orange dashes for 50%, and green dash-dotted for 90%. With increased $x - y$ velocity of the particles, the Lagrangian radii of each cluster remain constant. This velocity increase also produces an anisotropic velocity dispersion, with a lower value in the direction parallel to the filament (z direction, green line). In more massive models, the difference between σ_z and $\sigma_{x,y}$ decreases, as the dynamics of more massive models are less dominated by the gas potential, as expected.

there is no longer a cluster of stars, only streams of particles moving around the gas potential. Filaments with large maximum velocities will cross the cluster quickly, and the potential will not have enough time to accelerate the cluster. Hence, the cluster remains close to its initial position. With these quick passages, the filament cannot inject enough energy to completely destroy the cluster, so the it will be able to keep a small, but not zero, fraction of stars.

4.1 Outcomes for the clusters

For each pair of amplitude and period, we obtain objects with different fractions of particles inside the filament and inside the cluster. Figure 4 shows the position of the resulting object in this outcome space, where each point represents a different combination of oscillation parameters. The different symbols indicate the results for models A (blue plusses), B (orange dots), C (green crosses), and D (red stars). The masses and radii of these models are shown in Table 1. The black dashed line represents a 1:1 ratio between the fraction of particles left in the filament and in the cluster. After one oscillation, most of the remnants are located near this reference line. For models near this reference line, this can be explained by the fact that when a particle leaves the filament, it will also be ejected from the cluster, so the fraction of particles in the cluster will follow closely the fraction in the filament. However, the opposite is not necessarily true: a particle can leave the cluster by moving along the filament,

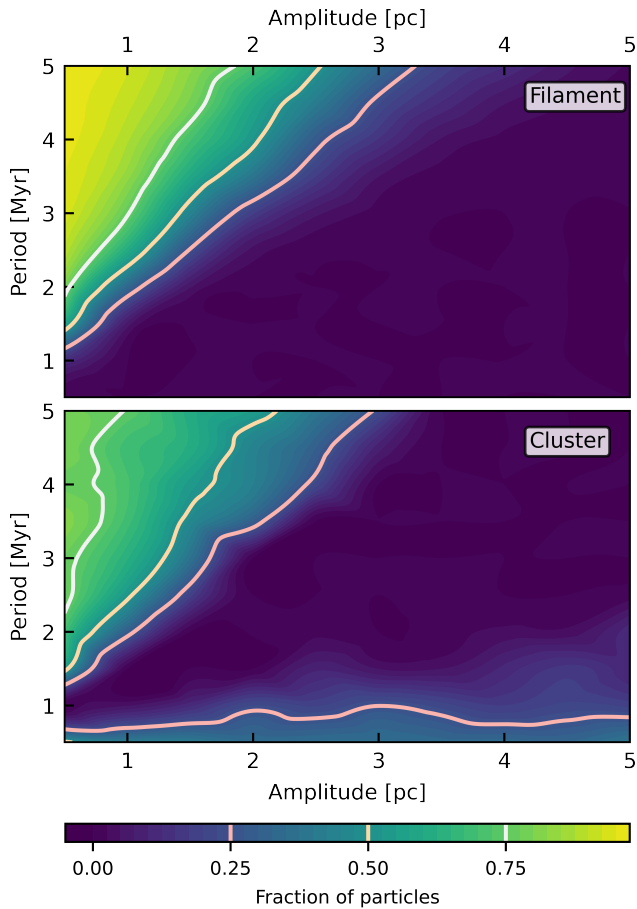


Figure 3. Fraction of particles left in the filament (top) and in the cluster (bottom) for different combinations of oscillation amplitude and oscillation period for Model A ($R_{\text{pl}} = 0.1$ pc, $M_{\text{pl}} = 250 M_{\odot}$). The color code indicates the fraction of particles after one full oscillation, with contours for 25%, 50% and 75% of the initial number of particles. The fraction in the filament decreases smoothly as the maximum velocity of the filament increases. A similar trend is observed for the fraction of particles in the cluster, with an increase in the number of particles if the filament is moving with a large velocity.

in which case said particle will be counted as “in the filament” but not as “in the cluster”, so the fraction in the filament tends to be slightly larger than the fraction in the cluster. Along this sequence we can identify three different outcomes for the cluster, plus a fourth type of object located outside the 1:1 line, this fourth type maintains most of the particles inside the cluster, and almost none inside the filament, indicating that the cluster has left the central part of the gas column. We name these types as 1) Filament Associated clusters; 2) transition clusters; 3) destroyed clusters; and 4) ejected clusters.

Not all models generate remnants in all regions. For example, the set of $R_{\text{pl}} = 0.1$ pc and $M_{\text{pl}} = 1000 M_{\odot}$ models (set C in Table 1) does not have destroyed clusters, either they lose a small fraction of stars or eject the whole cluster, as can be seen by the absence of green crosses in the region marked by the number three in Figure 4, which corresponds to the destroyed clusters. This also can be seen by plotting which pairs of amplitude and period from Figure 3 give rise to remnants belonging to each of the four regions. Figure 5 is such example for models A (top) and C (bottom). Each of the regions is represented by a different colour, following the numbers used in Figure 4. Filaments with small amplitude oscillations and

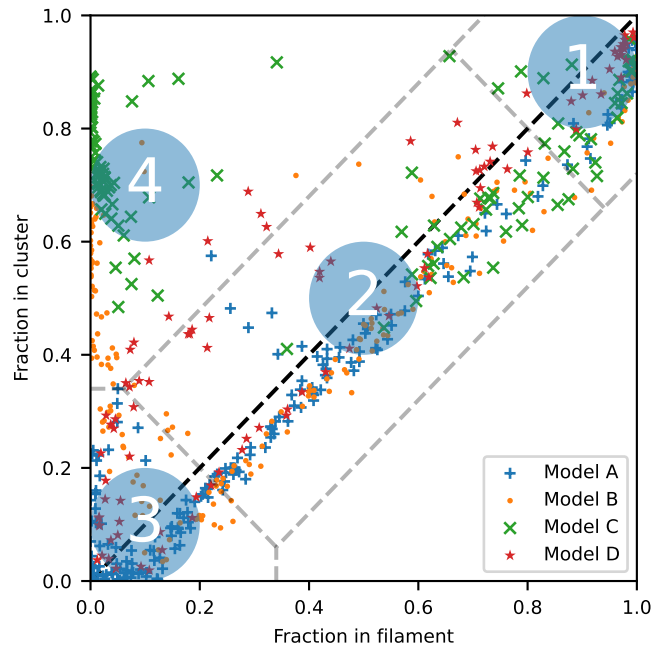


Figure 4. Fraction of particles in the cluster versus the filament at the end of the first oscillation for models with fixed $R_{\text{pl}} = 0.1$ (all models in sets A, B and C, plus model D, with $R_{\text{pl}} = 0.36$ pc, see Table 1). Each point in the plot corresponds to a simulation with different values of the oscillation amplitude and oscillation period. Each symbol represents a model, with blue pluses indicating simulations from Model A, orange dots for Model B, green crosses for Model C and red stars for Model D. We classify the remnant by its position in the fraction-fraction plot into one of four categories: 1) Filament Associated clusters, 2) Transition clusters, 3) Destroyed clusters, or 4) Ejected clusters (see main text for details on each category).

large periods are the ones that generate clusters for region 1, as mentioned above. As we use a filament with larger maximum velocity, the resulting remnant will be placed along the 1:1 track of Figure 4, generating objects in the transition region (region 2), then destroyed clusters (region 3), and finally generating ejected clusters (region 4).

If the filament is moving fast enough to eject the cluster, once the cluster moves outside the central part of the filament, its particles will still have the extra kinetic energy (see Section 2) but without the gas potential, the cluster will lose most of its stars until it is dissolved. On the other hand, for more massive clusters, the relative adjustment to the velocities that is required to maintain equilibrium in the filament is small compared to the velocities that the stars would have in the absence of the filament potential (see e.g. Figure 2). Hence, upon ejection from the filament, the stars remain, for the most part, bound to the cluster.

4.2 Filament Associated Clusters

Filaments with low amplitudes and large periods, which translates to low maximum velocities and acceleration, give rise to clusters in the “Filament Associated Cluster” region. They evolve in a similar way to clusters inside static filaments (Section 3), with relatively constant velocity dispersion, Lagrangian radii, and elongation along the filament. Figure 6 shows nine snapshots of model A ($R_{\text{pl}}=0.1$ pc, $M_{\text{pl}}=250M_{\odot}$), inside a filament oscillating with period $P=3.5$ Myr and amplitude $A=0.93$ pc. These snapshots cover a total of two full oscillations of the filament. The cluster always stays close to the filament.

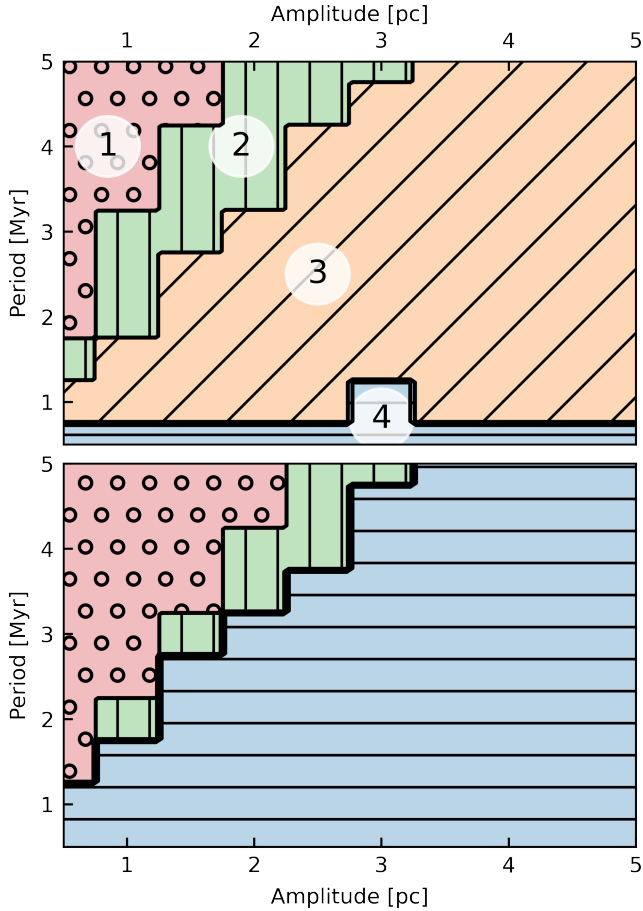


Figure 5. Classification of the remnants as function of the oscillation amplitude and period for models A (top) and C (bottom). The coloured regions and the numbers correspond to the numbered zones from Figure 4, with the red circles indicating the Filament Associated clusters, green vertical bars for the transition clusters, orange diagonal bars for the destroyed clusters, and blue horizontal bars for the ejected clusters. Note that model C does not have destroyed clusters for any combinations of oscillation period and amplitude.

At the beginning of the simulation, the cluster has zero mean velocity. As soon as the filament moves, the cluster starts to fall towards the centre of the filament. Due to the random motions of the particles, a fraction of these particles will have velocities with the opposite direction to the movement of the filament. The sum of these two effects, the cluster falling towards the filament, moving in the positive x direction, and the particles moving in the negative direction, is the cause of the initial ejection of particles, which can be seen in Figure 7, top panel. Even though the motion of the filament in the “Filament Associated Cluster” region cannot eject a large fraction of particles on its own, as reflected in the almost constant value of the fraction of particles in the filament of Figure 7, still some mass is lost due to the previously mentioned mechanism. Since the cluster is inside the filament, particles leave the cluster by moving in “corkscrew” orbits around the centre of the gas potential. This explains the downwards trend in the number of particles in the cluster, but constant fraction in the filament: particles leave the cluster, but they are unable to escape the filament.

The second panel in Figure 7 shows the mean velocity of the cluster for the three spatial axes. The cluster starts with zero velocity, but it is attracted by the moving potential, quickly falling back into the ridgeline of the filament. It is during this moment when most of

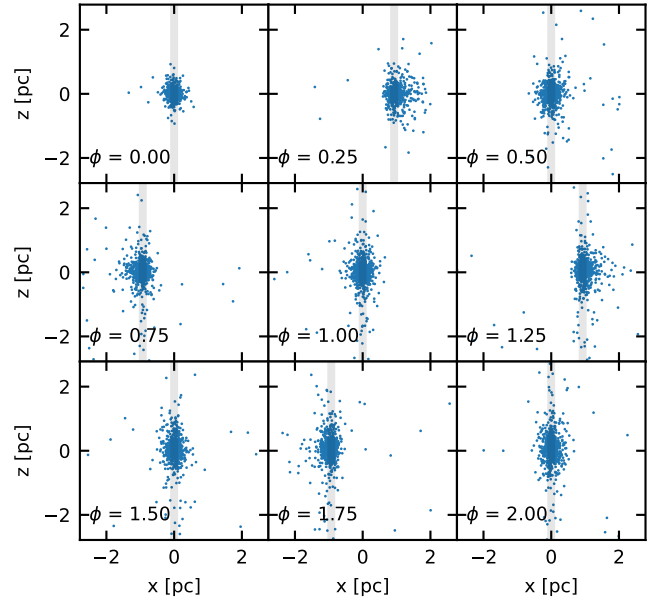


Figure 6. Time evolution of the stars (blue dots) in an oscillating gas filament (grey vertical line). The cluster shown here corresponds to model A ($R_{pl}=0.1$ pc, $M_{pl}=250M_{\odot}$), inside a filament that oscillates with period $P=3.5$ Myr and amplitude $A = 0.93$ pc. The slow movement of the filament is not enough to eject a significant fraction of particles from the cluster, and so we classify this cluster in the “Filament Associated Cluster” category. The label indicates the oscillation phase, defined as $\phi = t/P$, where $\phi = 1$ is the end of the first oscillation.

the ejections that the cluster experiences take place. After that initial acceleration phase, the cluster will move at the same velocity as the filament for the rest of the simulation.

4.3 Transition Clusters

Increasing the maximum velocity of the filament, either by increasing the oscillation amplitude, or by reducing the oscillation period, will increase the number of particles lost by the filament and by the cluster. This becomes evident after inspecting snapshots of this type of remnant. Figure 8 shows one example of a filament that produces a remnant in the transition region (region 2 from Figure 4), where we can see that a larger number of particles are ejected at $\phi = 0.25$ (Figure 8, second panel) when we compare with the remnant from Section 4.2. These snapshots correspond to a filament with amplitude $A = 0.74$ pc and period $P = 1.73$ Myr and a cluster with a total mass of $500 M_{\odot}$ and a Plummer radius of 0.1 pc (model B).

Clusters in this zone eject a considerable fraction of their initial mass, but leave a remnant that stays inside of the filament. Since the cluster stays inside the filament, once a particle leaves the filament, it also leaves the cluster. The opposite is not true: a particle can move along the filament and reach a distance larger than $5 R_{pl}$ from the centre of density of the cluster, and once it crosses that boundary, it is no longer counted as belonging to the cluster, but it is still inside the filament. This is the reason why “transition” clusters are located under the diagonal line in Figure 4, which acts as a reference for a 1 : 1 mass loss ratio, meaning that clusters in this zone have slightly more particles in the filament than in the cluster. Like clusters in a static filament (Section 3), or in the “Filament Associated Cluster” (Section 4.2) category, they are elongated in the direction of the filament (Figure 8, second panel onwards).

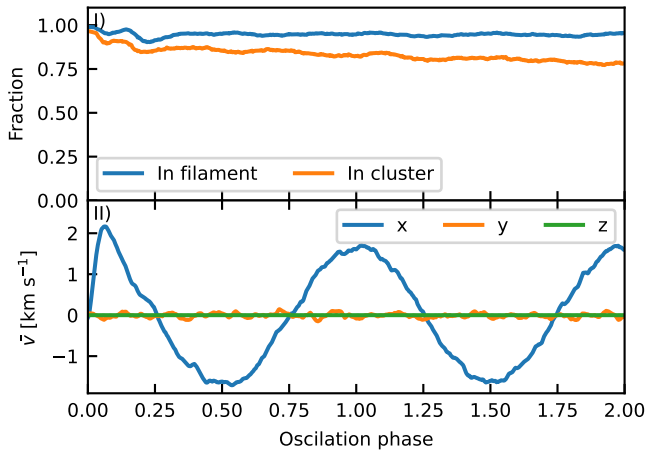


Figure 7. Time evolution of fraction of particles inside the cluster and inside the filament, and mean velocity of the particles for the simulation shown in Figure 6, which belongs to the “Filament Associated” clusters category. The top panel shows the fraction of stars inside the filament (blue line) and inside the cluster (orange line), as function of the oscillation phase. Second panel shows the mean velocity of the particle system for the three spatial directions (blue for x , orange for y , and green for z). The x axis, “Oscillation phase” corresponds to the quantity t/P , where P is the period of the oscillating filament.

For remnants in the “transition” region, we can clearly distinguish two phases of mass loss (Figure 9, first panel): the first phase occurs right at the beginning of the simulation, when the cluster starts to move towards the filament, and the second phase when the filament reaches its maximum distance from its initial position, causing the cluster to stop moving (to the right side in Figure 8) and ejecting the second group of stars. The first group of ejected stars corresponds to a small fraction of particles located mainly in front of the filament. These particles will attempt to fall into the cluster and into the filament, moving in opposite direction to the filament, and so are left behind the main bulk of stars (Figure 10, left panel). The second group of ejected stars follow a similar process, but they stay closer to the filament than the first group, and leave the cluster once the filament starts to recede back to its initial position (Figure 10, right panel). For both groups, once the ejected stars reach and cross the filament, they are moving too fast to be recaptured either by the filament or by the cluster. After the ejection of the second group of stars, the fraction of particles in the cluster remains constant during the remainder of the simulation, with only a handful of particles being ejected each time the filament reaches its maximum displacement (Figure 9, top panel).

The motion of the filament drags the particles only in the x direction. This translates to almost zero mean velocity in the y and z direction, as can be clearly seen in Figure 9, lower panel. The cluster starts at rest, but as it accelerates due to the motion of the filament, it reaches a maximum velocity of $\sim 3.0 \text{ km s}^{-1}$, larger than the maximum velocity of the filament. To better study the movement of the particles, we divide the particle system in two groups: the group of particles that are inside the filament by the end of the simulation, and the group of ejected stars. Figure 11 shows the mean velocity of the particles in the filament as the blue line, the ejected particles as the orange dashed line. Particles inside the filament clearly follow the gas potential, and move with the same velocity of the gas. In contrast, to the “destroyed” (see below) case, where the few particles that manage to stay inside the cluster are the ones that begin the simulation moving with velocities close to the one of the filament,

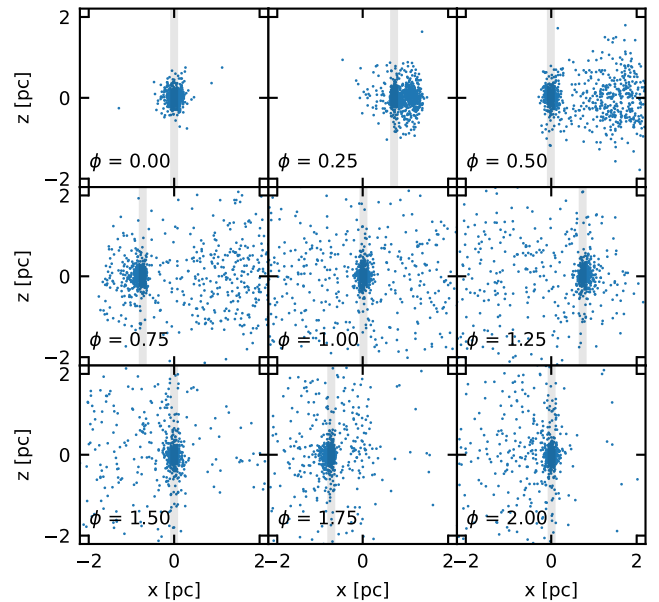


Figure 8. Time evolution of the stars (blue dots) in an oscillating gas filament (grey vertical line). The cluster shown here corresponds to model B ($R_{\text{pl}}=0.1 \text{ pc}$, $M_{\text{pl}}=500M_{\odot}$), inside a filament that oscillates with period $P=1.73 \text{ Myr}$ and amplitude $A = 0.74 \text{ pc}$. Compared with the previous case (Section 4.2), this model loses a larger fraction of particles at the first quarter of oscillation ($\phi = 0.25$), but still retaining more than 20% of the initial number of particles and, therefore, we classify it in the “transition” category (region 2 in Figure 4).

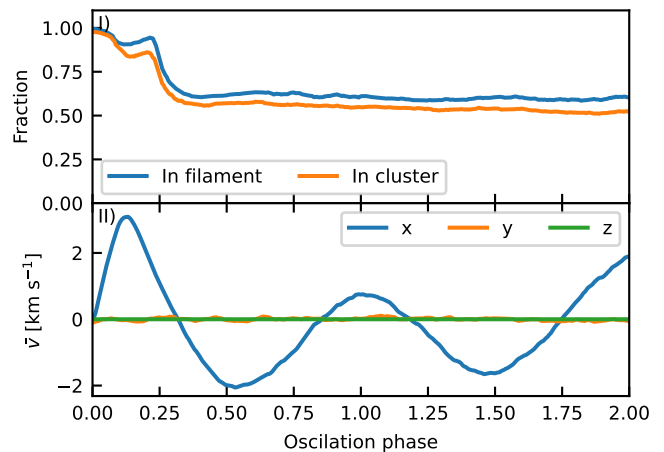


Figure 9. Same as Figure 7, for Model B and the parameters from Figure 8 (“transition” cluster). The top panel shows the fraction of stars inside the filament (blue line) and inside the cluster (orange line), as function of the oscillation phase. Second panel shows the mean velocity of the stars for the three spatial axis.

in the “transition” clusters, the particles inside the filament begin the simulation with lower mean velocities, but still moving in the same direction of the filament. When these particles cross the filament, they reach a maximum velocity that is larger than the maximum velocity of the filament, but remain bounded to the central part of the potential nonetheless. On the other hand, particles that are ejected are, on average, moving against the filament at the moment when the simulation starts. By the time these particles cross the filament, not only they are moving even faster than the maximum velocity of the

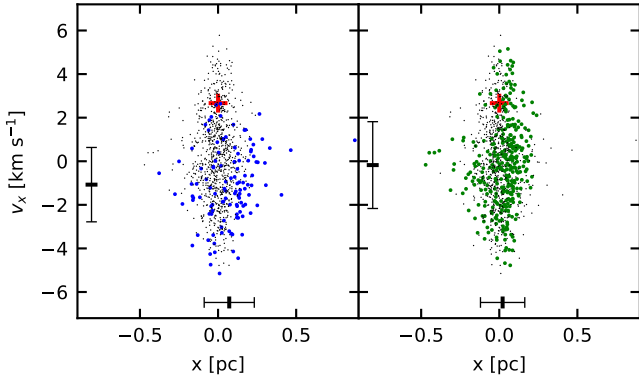


Figure 10. Phase space diagram showing the groups of stars ejected at the beginning (blue, left panel) and at turnaround (green, right panel) of the oscillation. The position and velocity of the filament represented with a red cross. The x axis corresponds to the direction of the filament oscillation. This snapshot corresponds to a cluster from model B ($R_{\text{pl}}=0.1$ pc, $M_{\text{pl}}=500M_{\odot}$), with the filament oscillating with $A = 0.74$ pc, $P = 1.73$ Myr. The bars at the left and bottom sides of the plot show the mean velocity and position of the highlighted particles relative to the filament, plus the dispersion on their values. In general, the particles ejected at the beginning are in front of the filament, and moving back towards the cluster.

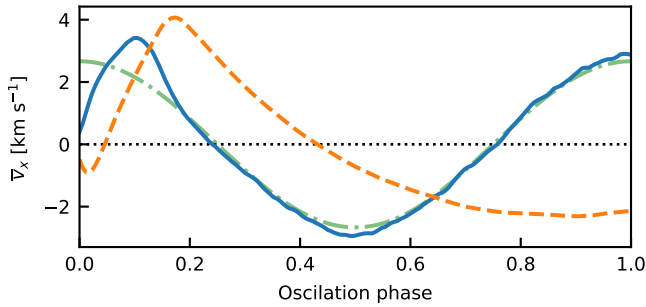


Figure 11. Mean velocity of the particles inside the filament (blue line) and of the ejected particles (orange dashed) for the simulation shown in Figure 8. The velocity of the filament is shown with the light green dash dotted line. As expected, the particles inside the filament move at the same velocity as the filament. On the other hand, the ejected particles have a larger maximum velocity than the particles inside the filament, which they reach at a later time. After that, the stirring of the filament causes the particles of this group to move in different directions, lowering their mean velocity.

bounded particles when they crossed the filament, they also reach the filament at a later time, so the difference in velocity between the stars and the gas is larger than for the previously mentioned group. The ejected particles do not cross the filament at the same time, nor with the same velocity. Therefore, they will reach different maximum distances from the filament, and will fall back at different times. An effect of the different fall back times is that while the particles that reach a larger distance from the centre of the simulation are starting to fall back into the filament, particles ejected with a low relative velocity are already being stirred by the filament and moving in the same direction (although not with the same velocity or at the same position, so it is unlikely that they will be recaptured) than the filament, so the mean velocity of this component of the system will maintain a low value.

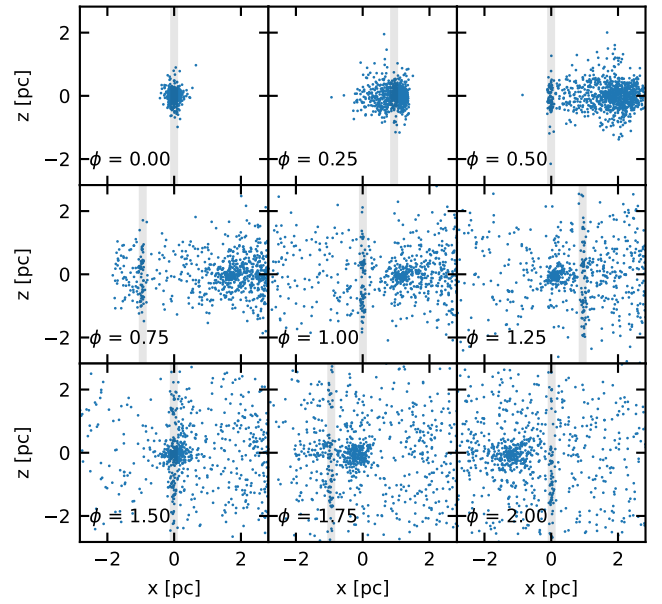


Figure 12. Time evolution of the particles (blue dots), representing stars, in an oscillating gas filament (grey vertical line). The cluster shown here corresponds to model B ($R_{\text{pl}} = 0.1$ pc, $M_{\text{pl}} = 500M_{\odot}$), inside a filament that oscillates with period $P=1.48$ Myr and amplitude $A = 0.94$ pc. This produces a remnant belonging to a destroyed cluster (region 3 in Figure 4) The small overdensity, visible from $\phi = 1.25$ onwards, is in fact two smaller clumps, created when the filament went through the main bulk of ejected stars at $\phi = 1.0$. These two associations have opposite v_y velocities, and they do not come together to form a new cluster.

4.4 Destroyed Clusters

Models in region 3 lose more than 80% of the particles within the first oscillation, and half of the initial mass is gone by the time the filament reaches its maximum distance from the initial position. The system has lost any resemblance of the original cluster, with streams of stars trying to catch up with the gas potential and only a few particles still in the central part of the filament (Figure 12). After most of the particles are dispersed, there is still a small overdensity left (Figure 12, middle row), which dissolves after subsequent filament crossings.

Figure 13, top panel, shows the catastrophic mass loss at the beginning of the simulation. As soon as the filament starts to move, approximately 25% of the particles leave the filament, only because they are moving with velocities in the opposite direction of the movement of the filament. The next phase of mass loss, bringing the fraction of particles inside the cluster from $\sim 75\%$ to its final $\sim 20\%$, corresponds to the moment when the filament reaches its maximum distance from its initial position. As the filament stops moving in the positive direction, and begins to move back into the centre of the simulation, the cluster is still moving with positive velocity (Figure 13, lower panel), too fast to be recaptured by the gas potential, and it will fly past the filament. Without the potential well of the gas, and stretched by the initial pull of the filament, the cluster is not able to keep its particles bounded any longer, leading to a steady decrease of the fraction of particles in the cluster. The ejected stars do not escape the filament and fall back into it (Figure 12, middle and bottom rows), explaining the almost constant fraction of particles in the filament at the end of the simulation in Figure 13, top panel.

Since most of the stars have been ejected, the mean velocity of the particles reflects the motion of the streams around the filament. Still, some stars move with the filament, so we can separate these

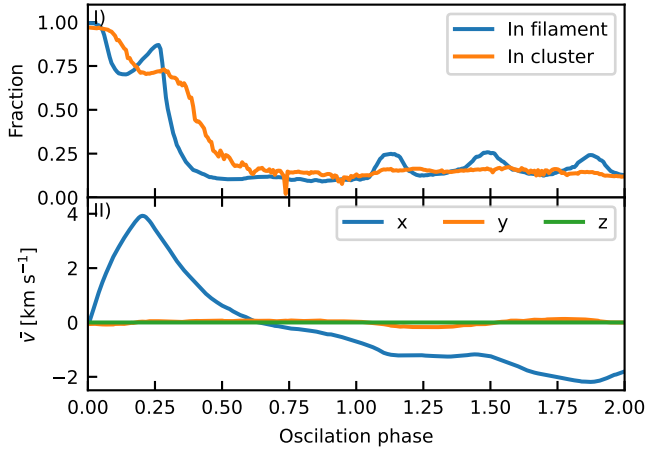


Figure 13. Same as Figure 7, for Model B and the parameters shown in Figure 12 (“destroyed” cluster). The cluster shown here corresponds to model B ($R_{\text{pl}}=0.1$ pc, $M_{\text{pl}}=500M_{\odot}$), inside a filament that oscillates with period $P=1.48$ Myr and amplitude $A=0.94$ pc. See caption of Figure 9 for an overview of each panel. The three bumps in the fraction of particles in the filament corresponds to the moment when the filament crosses the bulk of ejected particles.

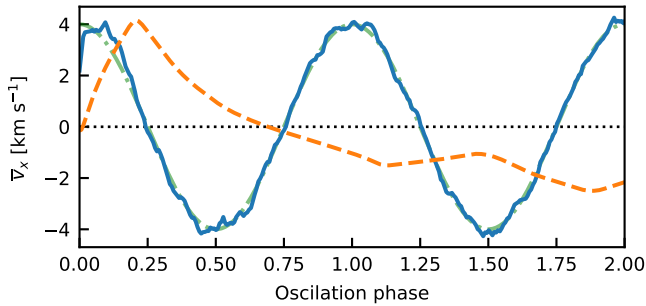


Figure 14. Mean velocity of the particles in the filament (blue line) and of the ejected particles (orange dashed) for the destroyed cluster of Figure 12. Similar to the behaviour noted in Section 4.3, the particles in the filament have the same velocity than the filament (green dash dotted).

two groups before measuring their mean velocities. In Figure 14, we select particles that are inside the filament at the end of the first oscillation and measure the mean velocity of the selected particles. It shows that the particles that manage to move with the filament are the ones that have initial velocities in the x direction close to the velocity of the filament, in contrast with the “Filament Associated” cluster (Section 4.2), where nearly all the particles manage to move with the filament, independently of their initial velocity. On the other hand, the bulk of the ejected particles re-enter the filament when the filament has stopped moving in the positive direction and is starting to turn back towards the centre of the simulation. At this moment, the particles are moving nearly as fast as the maximum velocity of the gas potential, and are ejected from the filament. The peak in velocity of Figure 14, top panel, at $\phi \sim 0.2$, and the secondary knees at $\phi \sim 1.1$ and $\phi \sim 1.8$ for the orange dashed line, mark the moment when the ejected particles cross the filament, which corresponds to the increments of the fraction of particles in the filament shown in the top panel of Figure 13.

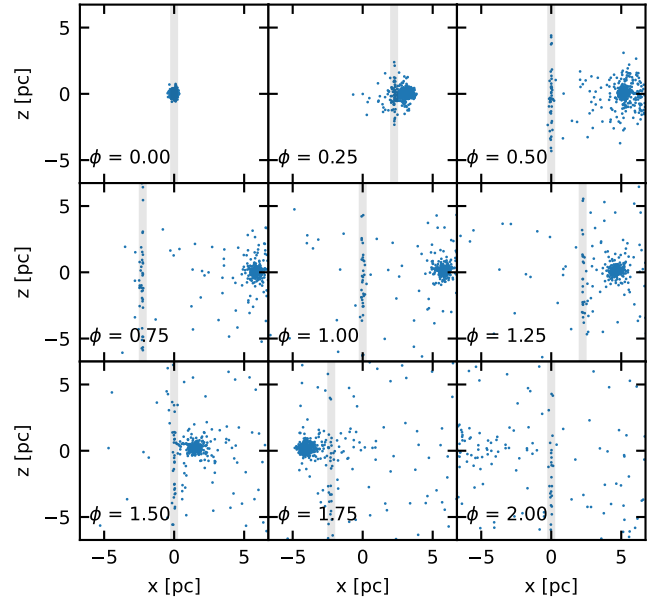


Figure 15. Time evolution of the stars (blue dots) in an oscillating gas filament (grey vertical line). The cluster shown here corresponds to model C ($R_{\text{pl}}=0.1$ pc, $M_{\text{pl}}=1000M_{\odot}$), inside a filament that oscillates with period $P=3.0$ Myr and amplitude $A=2.24$ pc. For this combination of oscillation period and amplitude, the cluster is ejected from the filament, reaching distances from the filament large enough to leave the plotting area ($\phi = 2.0$).

4.5 Ejected Clusters

As the name suggests, some clusters are ejected as a whole from the filament. That is, under some combinations of filament oscillation amplitude and period, the cluster escapes filament capture without losing enough mass to disrupt their equilibrium state. In other words, they have a potential well deep enough to survive removal from the gas filament. These models correspond to region 4 in Figure 4. One such example of an ejected cluster (model C, $R_{\text{pl}}=0.1$ pc, $M_{\text{pl}}=1000 M_{\odot}$) is shown in Fig 15.

As mentioned previously, formally our filament has an infinite mass when the density is integrated to $r \sim \infty$. This implies that these “escaped” clusters never actually escape the filament. Inevitably, they will succumb to gravity and fall back into the filament. However, in nature, we expect that the filament potential will not behave in this fashion, and depending on the mass of the filament versus the larger scale but still local ISM fluctuations these clusters will have a larger survival probability. That said, formally in our results and because of this infinite filament mass, even the “escaped” clusters will never truly escape the grasp of the filament potential. Hence they are inevitably trapped in an auto-destructive cycle of filament encounters, in which the number of times the cluster suffers a close and destructive filament encounter depends on the velocity of the cluster relative to the filament at the moment of first separation from the filament. Regardless of what happens in nature versus the artificial simulations, if the relative velocity is small, the cluster will on short order fall back into the filament, suffering multiple encounters and accompanying severe disruption of its structure. On the other hand, a high relative velocity at first separation will keep the cluster safe from filament-induced destruction for a longer time because of a reduced number of damaging encounters with the filament potential per unit time, or full escape from the local filament potential.

Similar to the clusters that fall in the category “destroyed” (Section 4.4), Figure 16 shows that “ejected” clusters also go through an

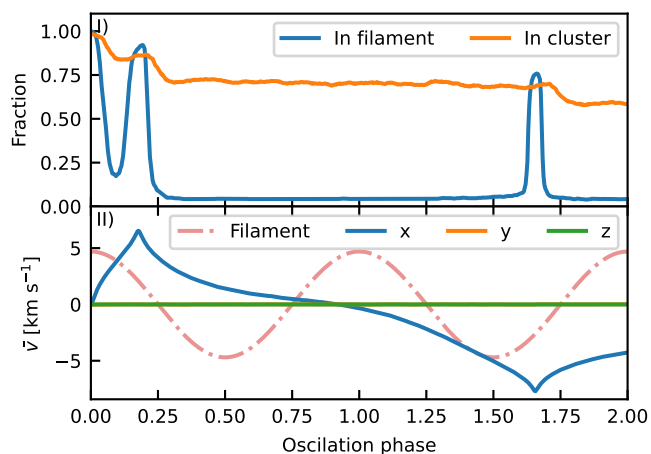


Figure 16. Same as Figure 7, but for Figure 15, “ejected” cluster. The cluster shown here corresponds to model C ($R_{\text{pl}} = 0.1$ pc, $M_{\text{pl}} = 1000M_{\odot}$), inside a filament that oscillates with period $P = 3.0$ Myr and amplitude $A = 2.24$ pc, which ejects the cluster at an oscillation phase of $\phi \sim 0.2$.

initial mass loss phase when the simulation begins (top panel) as the cluster starts to gain velocity to catch up with the moving filament. Particles in front of the filament, and with negative velocities, i.e. at the right side of the filament and moving to the left side in Figure 15, are the first particles that leave the cluster and are left behind by the filament. This represents around 10% of the initial mass of the cluster, and it is lost to the cluster before the filament reaches its maximum distance from the origin. There is a second phase of mass loss near the beginning of the simulation that corresponds to the moment when the cluster leaves the filament for the first time. This time, the particles that leave the cluster are the particles that begin the simulation with velocities close to the velocity of the filament; these particles stay inside the filament and are stripped from the cluster once the filament starts to recede back to its initial position. They follow the inevitable pull of the filament and are bound to it. After the second ejection, the cluster is outside the filament and moving away from it. As long as the cluster is outside the filament, it will not lose any more mass. Eventually, the cluster falls back into the filament, and will lose a fraction of its particles each time this happens.

As with the previous cases, the movement of the filament along the x axis induces the star system to have a mean velocity along the x direction. The cluster shown in Figure 15 accelerates from rest until it crosses the filament, shortly before the filament reaches its maximum distance from the centre of the simulation. At this moment, the cluster is moving at ~ 7.0 km s $^{-1}$ (Figure 16, bottom panel), ~ 4.5 km s $^{-1}$ faster than the filament. The crossing happens near the turn and, in consequence, the gas potential will not be able to slow down the cluster enough to recapture it, so the star system will overtake the filament. The cluster is able to reach a velocity larger than the maximum velocity of the filament. This can be explained with an observer moving with the filament. In the simulation frame, the cluster starts at rest, with $v_{\text{cl}} = 0$ km s $^{-1}$, while the filament is moving with $v_{\text{fil}}(t = 0) = v_{\text{max}}$. For the observer in the filament, at $t = 0$, it is the cluster what its moving away, with $v_{\text{cl}} = -v_{\text{max}}$, while the filament is static. As the simulation continues, eventually the cluster stops moving away and starts to fall back into the centre of the filament. At the moment of the filament crossing, the cluster will be moving with $v_{\text{cl}} = v_{\text{max}} + \delta v$, where δv is caused by the fictitious forces due to the acceleration of the filament in the simulation frame. Back in the simulation frame, the velocity of the cluster will be

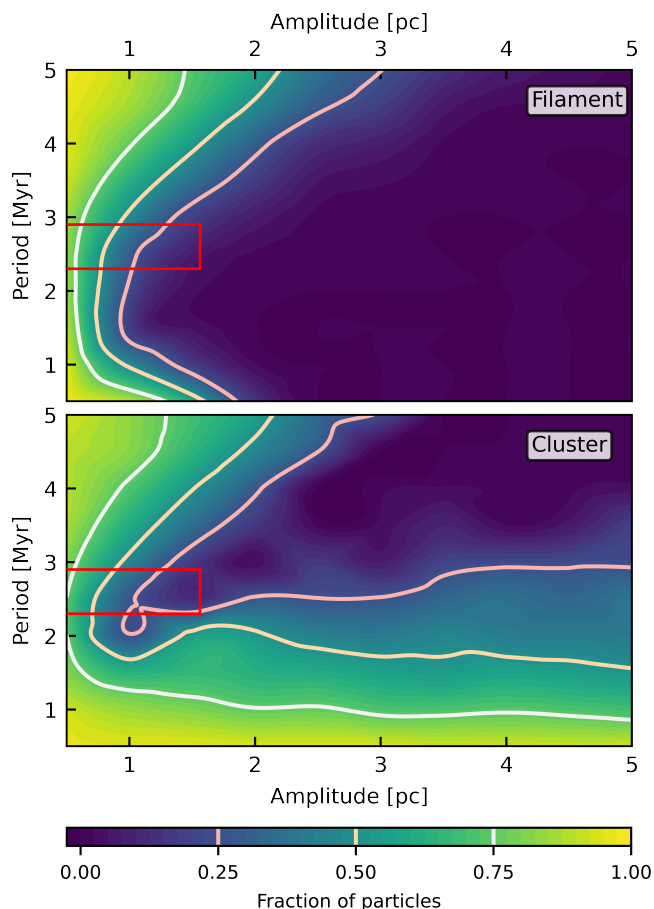


Figure 17. Fractions of particles in the filament (top) and in the cluster (bottom) for a model with radius and mass similar to the ONC. The red rectangle shows the possible oscillation parameters of the ISF, while the contours represent fractions of 25%, 50% and 75% of the initial particles.

$v_{\text{max}} + v_{\text{fil}}(t_{\text{encounter}}) + \delta v$, which will be larger than v_{max} , unless the encounter happens at a moment when $\delta v < -v_{\text{fil}}(t_{\text{encounter}})$. Then, as the filament recedes, the cluster starts to slow down, and reaching a maximum distance of 5.9 pc from its initial position. Once the cluster stops, it starts to fall back into the filament. Eventually, there is a new interaction between the gas potential and the star system, moment at which the cluster is, again, moving too fast to be captured by the filament. In this second interaction, the difference in velocity between the cluster and the filament is larger than in the first interaction: with the cluster moving at ~ 8.7 km s $^{-1}$, the velocity relative to the filament is ~ 6.1 km s $^{-1}$. This suggests that an ejected cluster could not only not be recaptured by the filament, it might gain enough velocity to escape the gas cloud that created it after a few crossings.

4.6 Orion Nebula Cluster

As our simulations have shown, the end state of the cluster depends on both, the parameters of the cluster and the parameters of the oscillation of the filament. For the case of the ONC, Stutz (2018) show that the cluster can be modelled as a Plummer sphere with a total mass of $1124 M_{\odot}$ and a Plummer radius of 0.36 pc. The fraction of particles left in the filament and in the cluster after one filament oscillation is shown in Figure 17, where we see that, indeed, there are regions in the period-amplitude plot that result in a destroyed cluster.

From the different pairs of period and amplitude, of special interest are the values that are close to the estimated oscillation parameters of the ISF (Stutz & Gould 2016; Boekholt et al. 2017; Schleicher & Stutz 2018; Stutz et al. 2018), shown in Figure 17 in the red rectangle. This suggests that, unless the oscillation has an amplitude smaller than the radial extent of the cluster, the ONC will lose a considerable fraction of stars and will be destroyed by the filament.

Observations of the ONC indicate that the cluster is in expansion (Jones & Walker 1988; Kroupa et al. 1999; Scally et al. 2005) and located slightly in the foreground of the ISF (Hillenbrand & Hartmann 1998; O'dell 2001). Under the slingshot scenario, these observations could indicate that the filament is close to its turnaround, and the cluster is being ejected from the filament, as already pointed out by Stutz (2018). Removing the gas from the cluster lowers the potential that is keeping the stars bounded together, causing the expansion of the cluster. Once outside the filament, the cluster is dissolved by the time the filament completes its second oscillation, so we expect a bleak future for the ONC, with this cluster being transformed to a smaller association of stars, or completely dispersing into the Galactic field.

5 DISCUSSION AND CONCLUSIONS

In this work we investigate the effects of an oscillating gas filament, also known as the Slingshot model, in the early evolution of a young star cluster. We achieve this via numerical simulations of a spherical distribution of particles inside a cylindrically symmetrical gas potential that oscillates with a sinusoidal motion. We are able to simulate the kinematics of the system by coupling an N-body solver with an analytical background potential.

Clusters in oscillating filaments will lose particles as soon as the simulation starts due to tides produced by the motion of the filament. The amount of ejected particles depends on the parameters of the cluster, the amplitude of the oscillation and the period of the oscillation.

The motion of the filament will cause the ejection of stars from the cluster. The majority of the ejected stars leave the filament when the filament reaches its maximum amplitude for the first time. The ejected particles move in the direction of the motion of the filament and eventually fall back into the filament.

We identify four outcomes for the cluster under the motion of the filament. We dub them as “Filament Associated”, “transition”, “destroyed” and “ejected” clusters, depending on the fraction of particles left inside the cluster and inside the filament. “Filament Associated Cluster” correspond to the clusters that remain inside the filament and keep at least 80% of their particles. On the other extreme, “destroyed” clusters are the remnants that keep at most 20% of their particles inside the filament and inside $5 R_{pl}$ from the centre of density of the star system. In the middle we have “transition” clusters, where a significant fraction of particles leave the cluster but there is still a clear overdensity of stars in the filament. Finally, “ejected” are, as the name implies, the clusters that are ejected by the motion of the filament and are not destroyed by the removal of the background potential. The fate of the cluster in an oscillating filament is decided quickly. By the time the filament reaches its maximum distance from its initial position, any star that manages to stay inside the cluster or the gas filament will likely stay there for the rest of the simulation time.

In a real cluster, stars would have different masses, which gives rise to processes of relaxation and mass segregation. As indicated in Section 2.3, we use equal mass particles in our simulations, so we do not observe such process. Although using a mass spectrum could

improve our results, the effects of the filament on the cluster take place in timescales shorter than the relaxation time of the clusters (Table 1). In the filaments with the largest period, the ejection or destruction of the cluster happens during the first 1.25 Myr (see Section 4.1), while the cluster with the shortest relaxation time, model C, has $t_{cr} = 1.21$ Myr. For filaments with shorter periods, the cluster does not have enough time to relax before the motion of the filament stirs the stars. On the other hand, Mouri & Taniguchi (2002) shows that the timescales for mass segregation are shorter than the relaxation time of the system, so mass segregation could be important in young systems. Observations show (Hillenbrand & Hartmann 1998; Allison et al. 2009; Pang et al. 2013; Plunkett et al. 2018; Dib & Henning 2019) that star clusters either form in a mass segregated state or reach mass segregation in a short timespan. In particular, the ONC is already mass segregated (Hillenbrand & Hartmann 1998). Since we consider that relaxation effects are not important in our simulations, and the study of mass segregation under the Slingshot model is outside the scope of this paper, we did not add a mass spectrum for our particles. Nonetheless, future numerical simulations could explore the effects of the Slingshot on the mass segregation process of young clusters.

According to Stutz (2018), the distribution of stars in the ONC is well characterized by a Plummer profile with a Plummer mass of $1124 M_{\odot}$ and a Plummer radius of 0.36 pc. A cluster with said parameters can be destroyed if the oscillation amplitude of the filament is larger than the radial extent of the cluster, given an estimated oscillation period of ~ 2.5 Myr.

ACKNOWLEDGEMENTS

The authors like to thank the anonymous referee for their comments, which helped to significantly improve the paper. DRMC, MCBMI and MF acknowledge financial support from Fondecyt regular No. 1180291. DRMC acknowledges funding through a beca Conicyt doctorado nacional convocatoria 2020. MF also acknowledges support by Conicyt Quimal No. 170001, and the ANID BASAL projects ACE210002 and FB210003. TCNB was supported by funds from the European Research Council (ERC) under the European Union’s Horizon 2020 research and innovation program under grant agreement No 638435 (GalNUC). AS gratefully acknowledges support from the ANID BASAL projects ACE210002 and FB210003. AS acknowledges support from the Fondecyt Regular (project code 1220610).

DATA AVAILABILITY

The data underlying this article will be shared on reasonable request to the corresponding author.

REFERENCES

- Allison R. J., Goodwin S. P., Parker R. J., Portegies Zwart S. F., de Grijs R., Kouwenhoven M. B. N., 2009, *MNRAS*, **395**, 1449
 André P., et al., 2010, *A&A*, **518**, L102
 Balega Y. Y., Chentsov E. L., Leushin V. V., Rzaev A. K., Weigelt G., 2014, *Astrophysical Bulletin*, **69**, 46
 Bally J., Langer W. D., Stark A. A., Wilson R. W., 1987, *ApJ*, **312**, L45
 Beccari G., et al., 2017, *A&A*, **604**, A22
 Binney J., Tremaine S., 2008, *Galactic Dynamics: Second Edition*
 Boekholt T. C. N., Stutz A. M., Fellhauer M., Schleicher D. R. G., Matus Carrillo D. R., 2017, *MNRAS*, **471**, 3590
 Casertano S., Hut P., 1985, *ApJ*, **298**, 80

- Clarke S. D., Whitworth A. P., Duarte-Cabral A., Hubber D. A., 2017, *MNRAS*, **468**, 2489
- Da Rio N., Robberto M., Hillenbrand L. A., Henning T., Stassun K. G., 2012, *ApJ*, **748**, 14
- Da Rio N., Tan J. C., Jaehnig K., 2014, *ApJ*, **795**, 55
- Da Rio N., et al., 2017, *ApJ*, **845**, 105
- Dib S., Henning T., 2019, *A&A*, **629**, A135
- Fűrész G., Hartmann L. W., Megeath S. T., Szentgyorgyi A. H., Hamden E. T., 2008, *ApJ*, **676**, 1109
- Foster J. B., et al., 2015, *ApJ*, **799**, 136
- Fujii M., Iwasawa M., Funato Y., Makino J., 2007, *PASJ*, **59**, 1095
- González Lobos V., Stutz A. M., 2019, *MNRAS*, **489**, 4771
- Großschedl J. E., et al., 2018, *A&A*, **619**, A106
- Hacar A., Tafalla M., Alves J., 2017, *A&A*, **606**, A123
- Hartmann L., Burkert A., 2007, *ApJ*, **654**, 988
- Hillenbrand L. A., 1997, *AJ*, **113**, 1733
- Hillenbrand L. A., Hartmann L. W., 1998, *ApJ*, **492**, 540
- Jones B. F., Walker M. F., 1988, *AJ*, **95**, 1755
- Kainulainen J., Stutz A. M., Stanke T., Abreu-Vicente J., Beuther H., Henning T., Johnston K. G., Megeath S. T., 2017, *A&A*, **600**, A141
- Kim D., Lu J. R., Konopacky Q., Chu L., Toller E., Anderson J., Theissen C. A., Morris M. R., 2019, *AJ*, **157**, 109
- Kounkel M., et al., 2018, *AJ*, **156**, 84
- Kroupa P., Petr M. G., McCaughrean M. J., 1999, *New Astron.*, **4**, 495
- Kroupa P., Aarseth S., Hurley J., 2001, *MNRAS*, **321**, 699
- Kroupa P., Jeřábková T., Dinnbier F., Beccari G., Yan Z., 2018, *A&A*, **612**, A74
- Lada C. J., Lada E. A., 2003, *ARA&A*, **41**, 57
- McMillan S., Portegies Zwart S., van Elteren A., Whitehead A., 2012, in Capuzzo-Dolcetta R., Limongi M., Tornambè A., eds, *Astronomical Society of the Pacific Conference Series Vol. 453, Advances in Computational Astrophysics: Methods, Tools, and Outcome*. p. 129 ([arXiv:1111.3987](https://arxiv.org/abs/1111.3987))
- Mouri H., Taniguchi Y., 2002, *ApJ*, **580**, 844
- O'dell C. R., 2001, *ARA&A*, **39**, 99
- Pang X., Grebel E. K., Allison R. J., Goodwin S. P., Altmann M., Harbeck D., Moffat A. F. J., Drissen L., 2013, *ApJ*, **764**, 73
- Pelupessy F. I., van Elteren A., de Vries N., McMillan S. L. W., Drost N., Portegies Zwart S. F., 2013, *A&A*, **557**, A84
- Plummer H. C., 1911, *MNRAS*, **71**, 460
- Plunkett A. L., Fernández-López M., Arce H. G., Busquet G., Mardones D., Dunham M. M., 2018, *A&A*, **615**, A9
- Portegies Zwart S., Bédorf J., 2014, arXiv e-prints, p. [arXiv:1409.5474](https://arxiv.org/abs/1409.5474)
- Portegies Zwart S., McMillan S., 2018, *Astrophysical Recipes; The art of AMUSE*, doi:10.1088/978-0-7503-1320-9.
- Portegies Zwart S., et al., 2009, *New Astron.*, **14**, 369
- Portegies Zwart S., McMillan S. L. W., van Elteren E., Pelupessy I., de Vries N., 2013, *Computer Physics Communications*, **184**, 456
- Proszkow E.-M., Adams F. C., Hartmann L. W., Tobin J. J., 2009, *ApJ*, **697**, 1020
- Reipurth B., Mikkola S., Connelley M., Valtonen M., 2010, *ApJ*, **725**, L56
- Scally A., Clarke C., McCaughrean M. J., 2005, *MNRAS*, **358**, 742
- Schleicher D. R. G., Stutz A., 2018, *MNRAS*, **475**, 121
- Seifried D., Walch S., 2015, *MNRAS*, **452**, 2410
- Stutz A. M., 2018, *MNRAS*, **473**, 4890
- Stutz A. M., Gould A., 2016, *A&A*, **590**, A2
- Stutz A. M., Kainulainen J., 2015, *A&A*, **577**, L6
- Stutz A. M., Gonzalez-Lobos V., Gould A., 2018, arXiv e-prints, p. [arXiv:1807.11496](https://arxiv.org/abs/1807.11496)
- Swiggum C., et al., 2021, *ApJ*, **917**, 21
- Takemura H., et al., 2021, *ApJ*, **910**, L6
- Theissen C. A., Konopacky Q. M., Lu J. R., Kim D., Zhang S. Y., Hsu C.-C., Chu L., Wei L., 2022, *ApJ*, **926**, 141
- Tobin J. J., Hartmann L., Fűrész G., Mateo M., Megeath S. T., 2009, *ApJ*, **697**, 1103
- Valtonen M., Karttunen H., 2006, *The Three-Body Problem*

This paper has been typeset from a $\text{\TeX}/\text{\LaTeX}$ file prepared by the author.